

# Performance assessment of photovoltaic/thermal hybrid adsorption-vapor compression refrigeration system

Mohamed G. Gado

Egypt–Japan University of Science and Technology (E-JUST), Energy Resources Engineering Department, New Borg El-Arab City, Alexandria, Egypt, mohamed.gado@ejust.edu.eg

Helwan University, Mechanical Power Engineering Department, Faculty of Engineering at El-Mattaria, P.O.11718, Cairo, Egypt

Shinichi Ookawara

Tokyo Institute of Technology, Department of Chemical Science and Engineering, Tokyo 152-8552, Japan, ookawara.s.aa@m.titech.ac.jp

Egypt–Japan University of Science and Technology (E-JUST), Energy Resources Engineering Department, New Borg El-Arab City, Alexandria, Egypt

Sameh Nada

Egypt–Japan University of Science and Technology (E-JUST), Energy Resources Engineering Department, New Borg El-Arab City, Alexandria, Egypt, sameh.nada@ejust.edu.eg

Hamdy Hassan

Egypt–Japan University of Science and Technology (E-JUST), Energy Resources Engineering Department, New Borg El-Arab City, Alexandria, Egypt, hamdy.aboali@ejust.edu.eg

Submitted: 02.10.2021

Accepted: 30.03.2022

Published: 30.06.2022



**Abstract:** Hybrid vapor compression systems based on adsorption are recognized as a viable alternative to traditional energy-intensive compression systems. Solar-powered hybrid adsorption-compression refrigeration systems feature a solar-powered silica gel/water-based adsorption cooling system paired with a traditional compression system that utilizes R134a as a refrigerant. Herein, the system feasibility of a solar-operated hybrid adsorption-compression refrigeration system has been evaluated theoretically using typical climatic data of Alexandria, Egypt. Mathematical modeling is generated and compared to the most relevant experimental data. PVT collectors are exploited to drive both the adsorption and the compression units. Simulation results suggest that using a three-to-one system size ratio between the adsorption and compression subsystems might considerably raise the COP from 2.9 to 5 for the compression system. It is observed that at an ideal size ratio of 7, the proposed system can considerably deliver an energy saving of 30.8 percent, compared to the hybrid system of the size ratio of 3, which attains only energy savings of 22.1 percent. Furthermore, the utilization of PVT collectors might feed the hybrid system by 3.474 kWh and augment the electric grid by 100 kWh, at an ideal size ratio of 7. Overall, investigating hybrid adsorption-compression systems might offer unique insight on optimizing the performance of conventional counterparts.

**Keywords:** Adsorption system, Compression system, Hybrid system, PVT

Cite this paper as: Gado, M. G., Ookawara, S., Nada, S., & Hasan, H., Performance assessment of photovoltaic/thermal hybrid adsorption-vapor compression refrigeration system. *Journal of Energy Systems* 2022; 6(2): 209-220, DOI: 10.30521/jes.1002871

© 2022 Published by peer-reviewed open access scientific journal, JES at DergiPark (<https://dergipark.org.tr/en/pub/jes>)

Nomenclature					
A	surface area, m <sup>2</sup>	is	isentropic	st	storage tank
A <sub>n</sub>	constants in Eq. (4)	k <sub>o</sub> , k <sub>1</sub> , k <sub>2</sub>	coefficients in Eq. (2)	sys	system
B <sub>n</sub>	constants in Eq. (4)	l	liquid state	T	temperature, K
con	condenser	M	mass, kg	t	time, s
COP	coefficient of performance (-)	max	maximum	U	overall heat transfer coefficient, kW m <sup>-2</sup> K <sup>-1</sup>
c <sub>p</sub>	specific heat capacity, kJ kg <sup>-1</sup> K <sup>-1</sup>	min	minimum	u	useful
cw	recooling water	m	mass flow rate, kg s <sup>-1</sup>	w	water
D <sub>s</sub>	surface diffusivity, m <sup>2</sup> s <sup>-1</sup>	N	compressor speed, r.p.m	wv	water vapor
D <sub>so</sub>	diffusion coefficient, m <sup>2</sup> s <sup>-1</sup>	out	outlet condition	VC	vapor compression
dbt	dry bulb temperature	p	pressure, kPa	V <sub>st</sub>	displacement volume, m <sup>3</sup>
des	desorption reactor; desorption	P	power, kW	<b>Greek Letter</b>	
E <sub>a</sub>	activation energy, kJ kg <sup>-1</sup>	Q	heat transfer rate, kW	η	efficiency, %
el	electric	q	instantaneous uptake, kg kg <sup>-1</sup>	β <sub>r</sub>	temperature coefficient, %
eva	evaporator	q*	equilibrium uptake, kg kg <sup>-1</sup>	<b>Subscript</b>	
exp	expansion device	r	reference	ads	adsorption reactor
H <sub>st</sub>	isosteric heat of adsorption, kJ kg <sup>-1</sup>	ref	refrigerant	chw	chilled water mixture
h <sub>fg</sub>	heat of vaporization, kJ kg <sup>-1</sup>	R <sub>u</sub>	universal gas constant, kJ kmol <sup>-1</sup> K <sup>-1</sup>	comp	electric compressor; vapor compression
HX	heat exchanger	R <sub>p</sub>	radius of adsorbent particle, m	<b>Abbreviations</b>	
hw	hot water	s	saturation	LDF	linear driving force
I	solar radiation, kW m <sup>-2</sup>	sg	silica gel	NOTC	nominal operating cell temperature
in	inlet condition	sr	sunrise	PVT	photovoltaic/thermal collector
int	intermediate	ss	sunset	RD	regular density

## 1. INTRODUCTION

Currently, refrigeration and air conditioning applications are crucial contributors to electricity usage, which make up 20% of the global consumed electricity [1]. Thus, enhancing the performance of a vapor compression system could play a vital role in diminishing the exerted electric power. Reducing the heat sink temperature of the compression facility is one of the approaches to improving the compression system's performance [2]. Therefore, using hybrid refrigeration systems to reduce the intermediate temperature could amend the baseline vapor compression refrigeration system's efficiency and harvest the inherent merits of the adsorption refrigeration systems, such as the operation flexibility with low driving temperatures and lack of corrosion crystallization [3]. The performance enhancement of adsorption cooling systems might be promoted using metal foams or nanofluids [4,5]. Moreover, using renewables to drive cooling/refrigeration systems is a promising alternative to reduce emissions of fossil fuels [4]. The concept of using an assisted cooling system-such as absorption or adsorption systems-to decrease the condensation temperatures of the vapor compression systems has been extensively elaborated by Gado et al [2]. Herein, the adsorption system is an alternative to the absorption system to cool down the compression system. This feature is mainly attributed to the inherent advantages of adsorption systems over their absorption counterparts. The rewards of using hybrid adsorption-compression systems:

- The operation for refrigeration application
- High operational flexibility
- Performance improvement and energy-saving potential
- Possibility to perform in accessible cooling mode

Palomba et al [6] examined different configurations of adsorption-compression hybrid systems, such as series, parallel and cascade connections. In this regard, outcomes proved that the attainable energy savings of a hybrid chiller could be enhanced at an escalated condenser/evaporator temperature differential. Similarly, Calise et al [6] proposed utilizing photovoltaic/thermal collectors to power a hybrid parallel-based adsorption-compression heat pump. Their findings revealed that this system could achieve an energy saving of 20% while having a payback period of 15 years. On the other hand, the entire combination of the adsorption-compression hybrid cycle by driving the adsorption unit and recovering the waste heat of the compression unit is scrutinized by Gibelhaus et al [7]. Their simulation results revealed that the most significant feasible energy saving is 22% for Athens, Greece.

Several authors have examined and developed the integration of adsorption refrigeration systems with compression systems for cascaded-type adsorption-mechanical integrated systems [8,9,10,11]. For instance, Vasta et al. [12] conducted experimental work on a hybrid adsorption-electric refrigeration system. Results ascertained that isobutane (R600a) and propane (R290) present superior performance than R717, R744 and R410A. Besides, Dino et al. [13] developed an experimental test rig to investigate the performance and potential energy savings of R1270-based adsorption-assisted hybrid compression arrangement. Their results demonstrated that such a hybrid system could achieve an electricity saving of up to 25%. Kilic and Anjrini [14] analyzed the performing indicators of a coupled adsorption-compression cycle using different working fluids, namely, R410A, R152A, R1234yf, R1270, and R32. Their results demonstrate that HFO-R1234yf can save electricity by about 65% compared with the used refrigerants. Gado et al [15] have explored the thermal and economic feasibility for different solar-powered adsorption-compression hybrid cooling layouts. One configuration is driven by ETC and photovoltaic panels for the adsorption and compression systems, respectively. In that configuration, the system entirely presents the concept of net-zero electricity. It was found that the system which utilizes only ETCs can attain an electricity saving of 64% per annum, compared to 100% presented by the latter configuration. Furthermore, the ETC/PV-based hybrid adsorption-compression cooling system achieved a 9.65-year payback period.

The advantages of combining an adsorption-based cooling system with a vapor compression refrigeration system may participate in; (i) operation for refrigeration applications compared to silica gel/water-based adsorption systems, (ii) running at low heat source temperatures without a considerable performance drop as opposed to conventional adsorption systems, and (iii) reducing electricity bills by utilizing hybrid systems in comparison with compression chillers, in particular at elevated condenser pressure. This study investigates the efficacy of a hybrid adsorption-based vapor compression refrigeration system driven by PVT collectors. Herein, PVT collectors cover the compression cycle's electric power with supplementary electricity production. PVT collectors are also used to provide thermal drive to the adsorption subsystem. Accordingly, for the sake of averting both the use of high-grade energy and dangerous repercussions on the environment of compression systems, it is compulsory to make use of solar-driven cooling systems. Consequently, utilization of these cooling systems can be a contributory factor in escalating the performance of the compression system by decreasing its intermediate temperature. Therefore, introducing solar-powered hybrid adsorption-compression refrigeration systems can contribute to energy savings and reduce detrimental ecological effects. Moreover, studying hybrid adsorption-compression systems opens new research avenues to optimize the performance of the prevalent compression cooling systems.

## 2. SYSTEM DESCRIPTION AND WORKING PRINCIPLES

Fig. 1 demonstrates the main components of the solar-driven integrated adsorption-vapor compression refrigeration system, which is composed of a photovoltaic/thermal-based solar system, a two-bed adsorption-based cooling system and a baseline compression (electric) refrigeration system. Herein, photovoltaic/thermal collectors are used due to their inherent advantages of providing both heat and electricity [16,17]. Silica gel/water pair is deployed in the adsorption refrigeration system, while R134a is adopted for the compression unit.

The cooling power of an adsorption facility approaches 12 kW, in which secondary fluid temperatures (generating, recooling, and chilled are 85°C, 30°C and 12°C, respectively), as opposed to a cooling power of a vapor compression refrigeration system (4 kW), which is appraised at secondary fluid temperature (recooling and chilled mixture temperatures of 30°C and -18°C, respectively). An ethylene glycol/water mixture is employed as a heat transfer fluid (HTF) to cover the product load of different applications, i.e., supermarkets and cold stores. The solar energy system comprises PVT collectors, which thermally drive the adsorption system and electrically power the vapor compression refrigeration system.

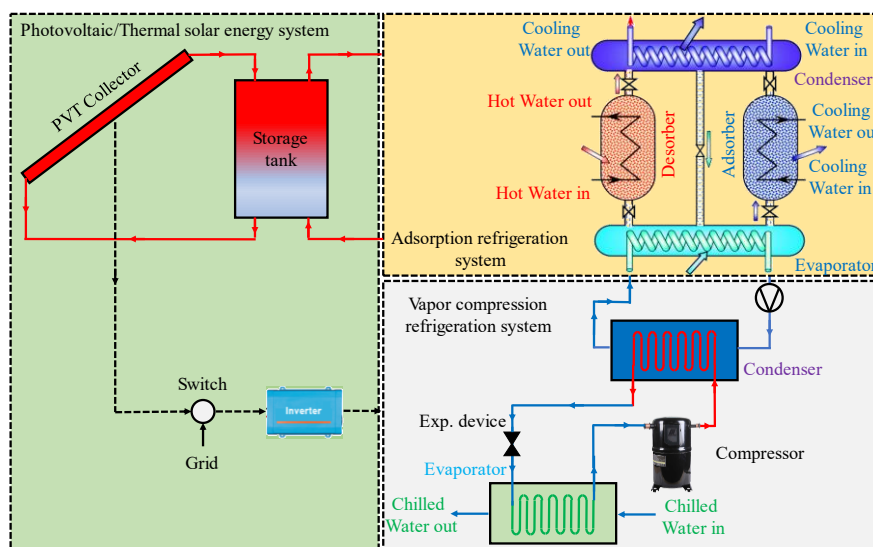


Figure 1. Integrated adsorption-compression refrigeration system coupled with PVT collectors.

### 3. MATHEMATICAL MODELING

#### 3.1. Solar Energy System

The daily global horizontal radiation and the ambient temperature of Alexandria city, Egypt is simulated as follows [18]:

$$\begin{cases} I(t) = I_{max} \sin\left(\frac{\pi(t - t_{sr})}{t_{ss} - t_{sr}}\right) \\ T_{dbt} = \left(\frac{T_{max} + T_{min}}{2}\right) - \left(\frac{T_{max} - T_{min}}{2}\right) \cos\left(\frac{\pi}{12}(t - 1)\right) \end{cases} \quad (1)$$

where, sunrise and sunset times, the maximum and minimum temperature, and maximum solar radiation are assigned by  $t_{sr}$  and  $t_{ss}$ ,  $T_{max}$ ,  $T_{min}$ , and  $I_{max}$ , respectively. Herein, it should be highlighted that the variation in the dry bulb temperature and solar radiation is correlated using Eq. (1) and based on invoked meteorological data from the National Aeronautics and Space Administration (NASA) database [1].

*Table 1. Average monthly maximum solar radiation, maximum and minimum dry bulb temperatures [1].*

Months	$t_{sr}$ (h)	$t_{ss}$ (h)	$I_{max}$ (W/m <sup>2</sup> )	$T_{max}$ (°C)	$T_{min}$ (°C)
January	6:53	17:34	472	18.4	9.1
February	6:28	17:57	565	19.3	9.3
March	5:50	18:18	700	20.9	10.8
April	5:16	18:38	813	24.0	13.4
May	4:57	18:59	872	26.5	16.6
June	4:59	19:08	944	28.6	20.3
July	5:16	18:56	960	29.7	22.8
August	5:35	18:24	947	30.4	23.1
September	5:53	17:46	868	29.6	21.3
October	6:14	17:12	723	27.6	17.8
November	6:40	16:57	556	24.1	14.3
December	6:58	17:07	455	20.1	10.6

For photovoltaic/thermal collectors, the electric and thermal characteristics can be assessed as [19]:

$$\begin{cases} (Mc_p)_{PVT} \frac{dT_{PVT}}{dt} = \eta_{PVT,th} I(t) A_{PVT} + \dot{m}_{PVT} c_{PVT} (T_{PVT,in} - T_{PVT,out}) \\ \eta_{PVT,th} = k_0 - k_1 \left(\frac{T_m - T_{dbt}}{I(t)}\right) - k_2 \left(\frac{(T_m - T_{dbt})^2}{I(t)}\right) \\ \eta_{PVT,el} = \eta_r [1 - \beta_r (T_{PVT} - T_r)] \\ P_{el} = \eta_{sys} \eta_{PVT,el} I(t) A_{PVT} \end{cases} \quad (2)$$

here for single-crystal (Mono-si) PVT collectors, reference efficiency represents  $\eta_r$  while  $\beta_r$  denotes the temperature coefficient for cell efficiency. The electric system efficiency ( $\eta_{sys}$ ) is about 0.80, which involves the efficiency of the inverter/converter component. Technical specifications of the PVT collectors are adapted from DualSun manufacturer [1]. In that regard, the empirical constants of the PVT collector, such as  $k_0$ ,  $k_1$  and  $k_2$ , denote the collector optical efficiency, the first-order loss coefficient, and the second-order loss coefficient, respectively, where their numerical values are 58.2%, 10.8 W/°C m<sup>2</sup> and 0 W/°C<sup>2</sup> m<sup>2</sup>, respectively [1]. Moreover, the reference conditions of the PVT collector (i.e., the reference temperature ( $T_r$ ) and the reference solar radiation) are taken as the standard test condition of 25 °C and 1000 W/m<sup>2</sup> [1].

### 3.2. Adsorption Cooling System

The mathematical modeling of the silica gel-based adsorption system is based on solving simultaneously the adsorption isotherm, the adsorption kinetics, mass and energy balance of the system's main components, namely, an adsorber-reactor, a condenser and an evaporator.

#### 3.2.1. Isotherms and kinetics of adsorption working pair

The adsorption/desorption rate of silica gel/water pair is governed by the linear driving force (LDF) model as follows [20]:

$$\frac{dq}{dt} = \frac{15D_{so} \exp\left(-\frac{E_a}{R_u T}\right)}{R_p^2} (q^* - q) \quad (3)$$

The main characteristics of silica gel/water pair are listed in Table 2.

Table 2. Operating constants of adsorption kinetics and isotherms [21].

Parameter	Description	Value
$R_p$	average radius of silica gel particle	0.17E-03 m
$R_u$	universal gas constant	8.314 kJ/kmol K
$D_{so}$	diffusion coefficient	2.54E-04 m <sup>2</sup> /s
$E_a$	activation energy	2330 kJ/kg
$H_{st}$	isosteric heat	2800 kJ/kg

The modified Freundlich equation can be used to correlate the adsorption isotherms of the RD silica gel/water pair, as shown below [21]:

$$q^* = \sum_{n=0}^3 A_n T_s^n \left[ \frac{p_s(T_w)}{p_s(T_s)} \right]^{\sum_{n=0}^3 B_n T_s^n} \quad (4)$$

Adsorption isotherms' constants of  $A_n$  and  $B_n$  are presented in Table 3. Also,  $T_s$  denotes the adsorbent material temperature.

Table 3. Constants of modified Freundlich correlation [22].

Parameter	Unit	Value	Parameter	Unit	Value
$A_0$	kg/kg	-6.5314	$B_0$	-	-15.587
$A_1$	kg/kg K	0.072452	$B_1$	1/K	0.15915
$A_2$	kg/kg K <sup>2</sup>	-0.23951x10 <sup>-3</sup>	$B_2$	1/K <sup>2</sup>	-0.50612x10 <sup>-3</sup>
$A_3$	kg/kg K <sup>3</sup>	0.25493x10 <sup>-6</sup>	$B_3$	1/K <sup>3</sup>	0.5329 x10 <sup>-6</sup>

#### 3.2.2. Heat balance

Based on lumped parameter modeling, the energy balance of the four main components of the adsorption system is assessed by [3]:

$$\left\{ \begin{array}{l} (M c_p)_{des} \frac{dT_{des}}{dt} = M_{sg} H_{st} \frac{dq_{des}}{dt} + \dot{m}_{hw} c_{hw} (T_{hw,in} - T_{hw,out}) \\ (M c_p)_{ads} \frac{dT_{ads}}{dt} = M_{sg} H_{st} \frac{dq_{ads}}{dt} + \dot{m}_{cw} c_{p,cw} (T_{cw,in} - T_{cw,out}) \\ (M c_p)_{con} \frac{dT_{con}}{dt} = -[M_{sg} h_{fg} + M_{sg} c_{p,wv} (T_{des} - T_{con})] \frac{dq_{des}}{dt} + \dot{m}_{cw} c_{cw} (T_{cw,in} - T_{cw,out}) \\ (M c_p)_{eva} \frac{dT_{eva}}{dt} = -[M_{sg} h_{fg} + M_{sg} c_{p,l} (T_{con} - T_{eva})] \frac{dq_{ads}}{dt} + \dot{m}_{int} c_{int} (T_{int,in} - T_{int,out}) \end{array} \right. \quad (5)$$

By retrieving the logarithmic mean temperature difference method, the outlet temperatures of adsorber reactor, desorber reactor, evaporator and condenser are calculated as follows [22,23]:

$$T_{HX,out} = T_{HX} + (T_{HX,in} - T_{HX}) \exp\left(\frac{-UA_{HX}}{\dot{m}_w c_w}\right) \quad (6)$$

The mass flow rate, the overall thermal conductance, and the thermal capacitance of the chief components are listed in Table 4.

### 3.2.3. Continuity balance

The quantity of refrigerant (water vapor) for the adsorption unit is estimated as follows [24]:

$$\dot{m}_{w,eva} = -M_{sg} \left[ \frac{dq_{ads}}{dt} + \frac{dq_{des}}{dt} \right] \quad (7)$$

here  $M_{sg}$  stands for the quantity of the adsorbent material (silica gel).

Table 4. The adsorption cooling system's implemented factors [14].

Factor	Explanation	Value (unit)
$M_{sg}$	mass quantity of silica gel per bed	47 kg
$(Mc_p)_{ads/des}$	thermal capacitance of the adsorber/desorber	71.055 kJ/K
$(Mc_p)_{con}$	thermal capacitance of the condenser	72.162 kJ/K
$(Mc_p)_{eva}$	thermal capacitance of the evaporator	214.106 kJ/K
$UA_{ads/des}$	overall thermal conductance of the adsorber/desorber	4.241 kW/K
$UA_{con}$	overall thermal conductance of the condenser	15.349 kW/K
$UA_{eva}$	overall thermal conductance of the evaporator	4.885 kW/K
$\dot{m}_{hw}$	hot water mass flow rate of the desorber	1.28 kg/s
$\dot{m}_{cw}$	cooling water mass flow rate of the adsorber/condenser	1.52/1.37 kg/s
$\dot{m}_{int}$	intermediate mass flow rate the condenser/evaporator	0.71 kg/s

### 3.3. Vapor Compression Refrigeration System

The heat balance for both the condenser/evaporator heat exchangers can be conveyed as follows [1]:

$$\begin{cases} (Mc_p)_{con} \frac{dT_{con}}{dt} = \dot{m}_{ref}(h_{comp,out}^{actual} - h_{exp,in}) + \dot{m}_{cw} c_{cw} (T_{int,in} - T_{int,out}) \\ (Mc_p)_{eva} \frac{dT_{eva}}{dt} = -\dot{m}_{ref}(h_{comp,in} - h_{exp,out}) + \dot{m}_{chw} c_{chw} (T_{chw,in} - T_{chw,out}) \end{cases} \quad (8)$$

It should be mentioned that the compressor undergoes an adiabatic process, while the refrigerant is isenthalpically expanded in the expansion device ( $h_{in} = h_{out}$ ). The electric power of the compressor and cycle mass flux are presented below [25]:

$$\begin{cases} P_{el} = \dot{m}_{ref}(h_{comp,in} - h_{comp,out}) \\ \dot{m}_{ref} = V_{st} \eta_v N \rho_{comp,in} \end{cases} \quad (9)$$

where  $V_{st}$ ,  $\rho_{comp,in}$  and  $N$  describe the displacement volume, compressor's inlet density and rotational speed of the compressor. These numerical values are listed in Table 5.

Table 5. Baseline specifications for the compression refrigeration system [12].

Parameter	Description	Value
$UA_{con}$	overall thermal conductance of the condenser	4.885 kW/K
$UA_{eva}$	overall thermal conductance of the evaporator	3.000 kW/K
$\dot{m}_{chw}$	chilled water mass flow rate of the evaporator	0.857 kg/s
$\eta_{is}$	isentropic efficiency of the compressor	0.85
$\eta_v$	volumetric efficiency of the compressor	$1 - 0.04 \left[ \left( \frac{P_{con}}{P_{eva}} \right)^{1/1.2} - 1 \right]$
$\eta_{el}$	electrical efficiency of the compressor	0.90

### 3.4. Performance Indicators

The thermal amalgamation of adsorption and compression subunits can be expressed using the energy balance between the compression unit's condenser and the evaporator of the adsorption unit. Besides, the size ratio of the coupled system can be given as follows [2]:

$$Q_{eva}^{ads} = Q_{con}^{comp} \quad (10)$$

$$Size\ Ratio\ (SR) = \frac{Q_{eva,ads}}{Q_{eva,VC}} \quad (11)$$

Hybrid COP, adsorption COP and energy savings (ES) are used here as performance indicators as expressed below [1]:

$$\left\{ \begin{array}{l} COP_{VC} = \frac{Q_{eva,VC}}{P_{el,VC}} \\ COP_{ads} = \frac{Q_{eva,ads}}{Q_{gen,ads}} \\ ES = \frac{P_{el,VC} - P_{el,hybrid}}{P_{el,VC}} \times 100 \end{array} \right. \quad (12)$$

## 4. RESULTS AND DISCUSSION

The developed mathematical model for the adsorption-compression hybrid refrigeration system is performed employing SIMULINK and REFPROP. The thermodynamic properties of the working fluids are invoked using sequential S-functions. Herein, ODE15s functions are utilized as a solver of ordinary differential equations. The hybrid system is driven by 60 PVTs (total aperture area of 98 m<sup>2</sup>). The total adsorption cycle repeats itself each quarter-hour, comprising preheating time, desorption time, precooling and adsorption times of 30 s, 420 s, 30 s and 420 s, respectively. The system performance is examined using the meteorological data for Alexandria, Egypt (Latitude of 31.2°N and Longitude of 29.9°E).

### 4.1. Model Validation

To confirm the mathematical model's reliability, adsorption and compression cycles are autonomously proven. In the adsorption system, the dynamic modeling of the system is validated with experimental figures of Saha et al. [23], as shown in Fig. 2. While, for the compression system validation, it is clear from Fig. 3 that an adequate consistency between the experimental and simulation results, the coefficient of performance has an average deviation of about 6.4 percent between predicted and experimental data [12].

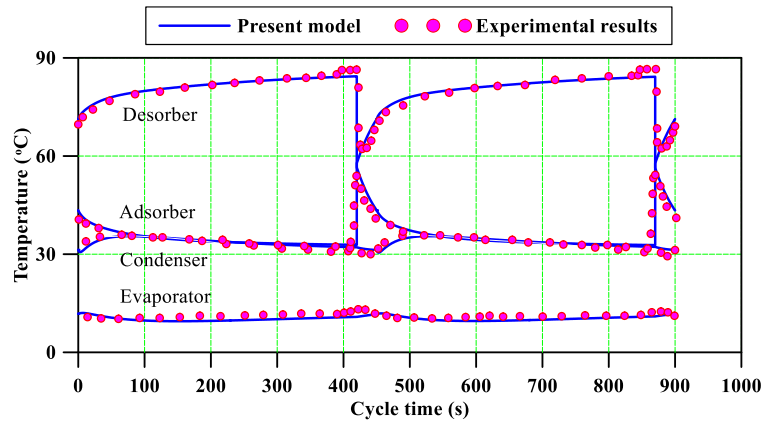


Figure 2. Resemblance of the mathematical model with experimental results of Saha et al. [23] for the adsorption system

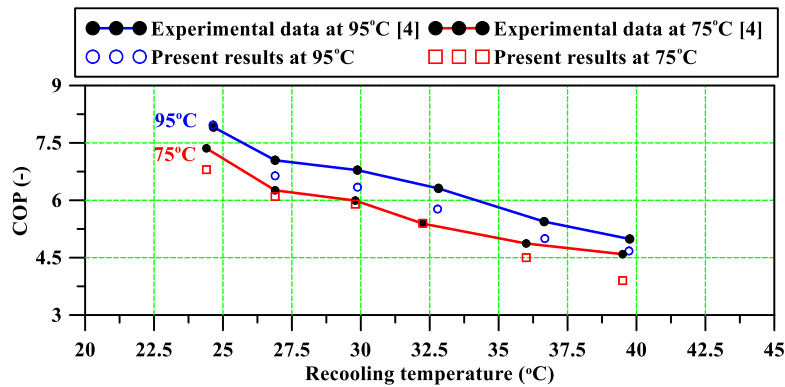


Figure 3. Mathematical model validation versus experimental findings of Vasta et al. [12] for the compression system

#### 4.2. Proper Integration and Heat Balance Verification

To envisage the thermal balance of the hybrid system operation, which is recognized by the energy equilibrium between the topping cycle (adsorption cycle) and the bottoming cycle (compression cycle), Eq. 10 is employed. This dynamic coincidence is exhibited in Fig. 4. By conspicuously revealing not only the discontinuity of the refrigeration capacity of the adsorption-based cooling system (dynamic behavior) compared with the approximately constant value of the condensation power for the compression system (steady-state behavior) but also the equivalence of the average values of this heat rate as recognized by Eq. 10.

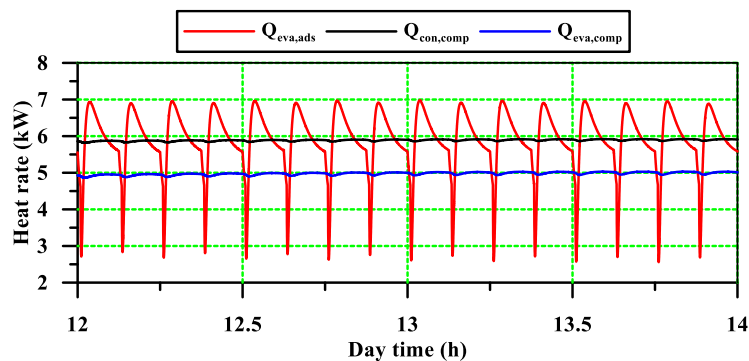


Figure 4. Variation in heat rate for the adsorption system's evaporator and the compression system's condenser and evaporator

### 4.3. Performance Investigation of the Hybrid System

Fig. 5 reveals the temperature histories of the chief elements of the suggested configuration, namely the adsorption system's elements: PVT collector, storage tank, desorber/adsorber reactors, condenser/evaporator units; and compression system's elements: condenser and evaporator. The temperature of the storage tank is given a driving temperature and varies according to the daily solar radiation and the thermal inertia of the solar system, while the recooling entry temperature quantifies 30°C. The chilled inlet temperature is taken as -18°C for the evaporator of the compression system. It can be observed from Fig. 5 that the storage tank temperature reaches its maximum value (~67°C) at 2 pm, which corresponds to a minimum intermediate temperature of ~13°C. This feature could significantly enhance the system performance of the prevalent compression system. Accordingly, the power demand drastically reduces when the intermediate temperature decreases to 13°C compared to the prevalent compression system, whose intermediate temperature is 30°C. Fig. 6 indicates that the minimum attainable compression power is 1.00 kW compared to 1.37 kW for the conventional system.

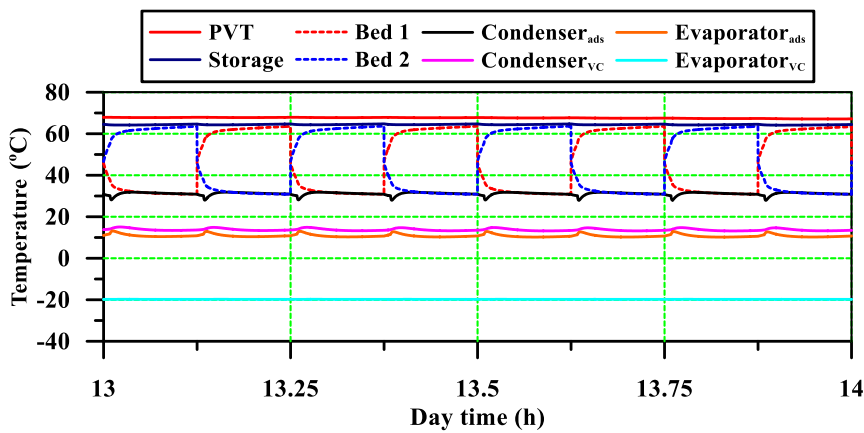


Figure 5. Temperature histories for the chief components of the hybrid system

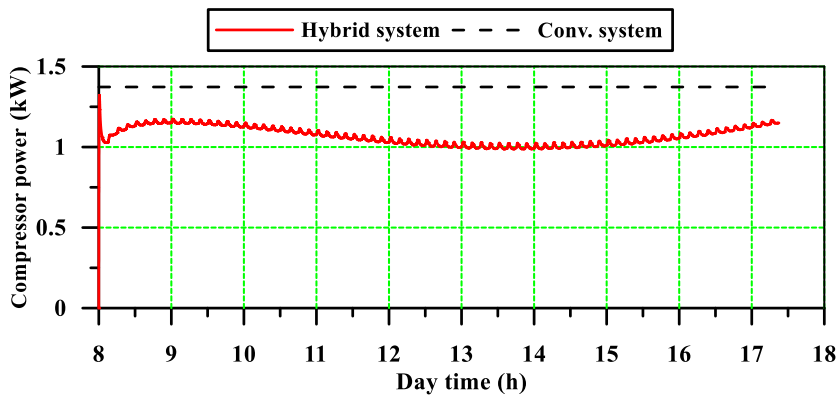


Figure 6. The compression power for the hybrid and the conventional systems

The COP for the conventional compression, the hybrid compression and the adsorption systems is indicated in Fig. 7. The cycle COP of the adsorption system increases to an average cyclic value of ~0.7. The higher value of the COP for the adsorption system might be attributed to the higher values of the evaporator pressure of the adsorption system (~13°C). In comparison, the COP of the hybrid system increases and then decreases, following the solar system radiation and the thermal inertia of the hot storage tank. It achieves a peak COP of 5 instead of the COP of 2.9 of conventional compression systems. Fig. 8 exhibits the daily resulted variation of the energy savings of the hybrid system during July using the meteorological data of Alexandria. It can be seen that the hybrid system could attain a maximum energy savings of 27% at 2 pm, which coincides with the peak driving temperature and minimum intermediate temperature. Overall, the hybrid system could achieve a daily average energy savings of 22.1%.

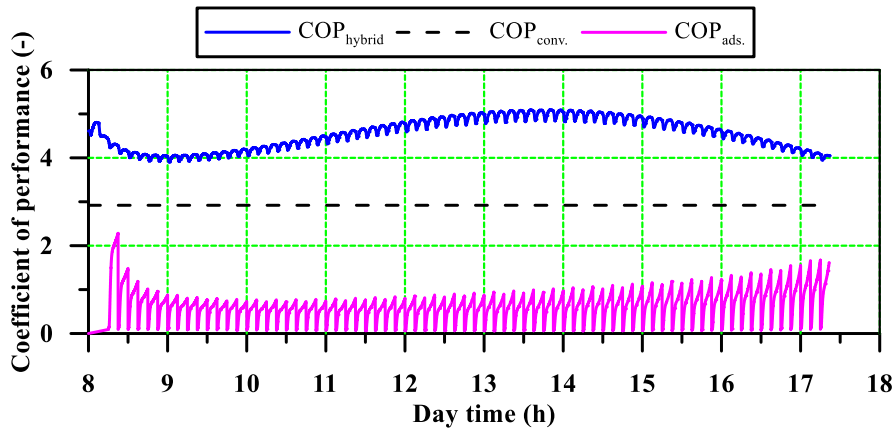


Figure 7. Variation of the cyclic performance metrics throughout the day

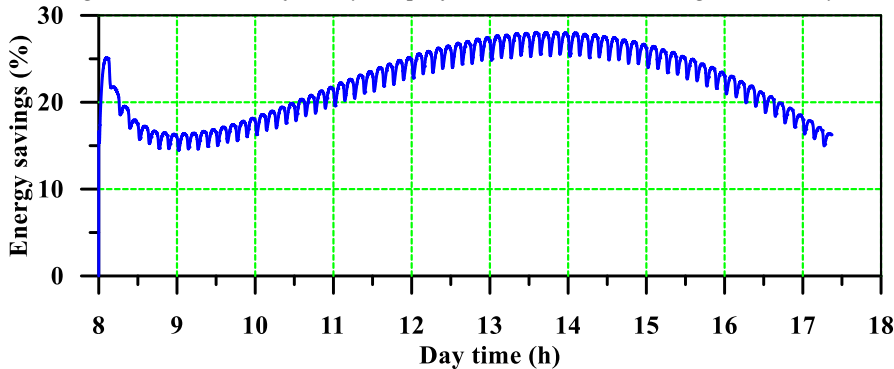


Figure 8. Variation of the cyclic energy savings throughout the day

#### 4.4. Optimum Matching and Proper Integration

The size ratio varies over a wide range (3:7) to achieve the proposed layout’s optimum performance. The SR is limited by the minimum possible evaporation temperature (5 °C), leading to better compression system performance. Fig. 9 shows that the maximum attainable energy savings (30.8%) are obtained at SR of 7, while SR of 3 attains minimum energy savings of 22.1%. Therefore, in this study, it is preferable to operate the system beyond SR of 7. Also, Fig. 10 exhibits the daily electricity production of PVT collectors for various size ratios between the adsorption and the compression systems, which are used basically to cover the required electricity of the hybrid system, and the remainder is fed to the electric grid. It can be observed that the SR of 7 could generate electricity of 103.3 kWh, which is used to cover the requisite electricity of the hybrid system (3.474 kWh). The surplus electricity of 100 kWh is supplied to the grid. It is worth mentioning that the SR of 3 requires 10 kWh to drive the hybrid system, and PVT collectors can produce 108 kWh.

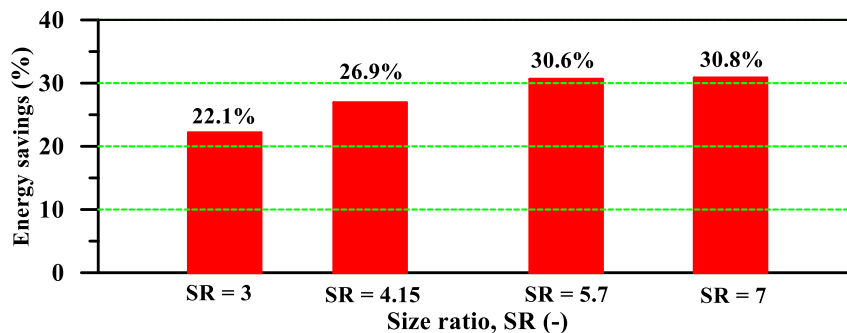


Figure 9. Energy savings for different proposed size ratios

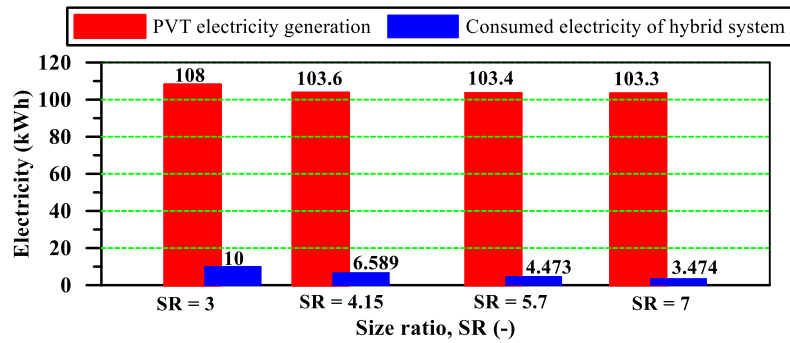


Figure 10. Electricity production and the needed electricity for the hybrid system at various size ratios.

## 5. CONCLUSION

A mathematical model is established and verified against experimental data from the literature. The influence of the size ratio is investigated to examine the performance metrics using COP and ES for the hybrid adsorption-compression refrigeration system. Based on the model key findings, the subsequent conclusion can be derived:

At a size ratio of 3, the hybrid system delivers a minimum compression power of 1.0 kW versus 1.37 kW for the conventional compression system.

Simulation results indicate that the hybrid system's highest COP is around 5, compared to 2.9 for a compression system, and that the maximum adsorption COP for SR of 3 is around 0.7.

Using SR of 3, the hybrid system can save 22.1% of electricity, and at an optimum SR of 7, it can save 30.8% of electricity.

To sum up, the amalgamation between adsorption and compression refrigeration systems could significantly improve the performance of conventional compression systems; therefore, such technology is worthwhile and promising for real applications of cooling and refrigeration systems.

## Acknowledgment

The authors are grateful for the scholarship, facilities, and tools provided by the Egyptian Ministry of Higher Education (MOHE) and the Egypt-Japan University of Science and Technology (E-JUST).

## REFERENCES

- [1] Gado, MG, Megahed, TF, Ookawara, S, Nada, S, El-Sharkawy, II. Potential application of cascade adsorption-vapor compression refrigeration system powered by photovoltaic/thermal collectors. *Applied Thermal Engineering* 2022; 207:118075. DOI:https://doi.org/10.1016/j.applthermaleng.2022.118075.
- [2] Gado, MG, Ookawara, S, Nada, S, El-Sharkawy II. Hybrid sorption-vapor compression cooling systems : A comprehensive overview. *Renewable and Sustainable Energy Reviews* 2021; 143: 110912. DOI:10.1016/j.rser.2021.110912.
- [3] Gado, M, Elgendy, E, Elsayed, K, Fatouh, M. Performance enhancement of an adsorption chiller by optimum cycle time allocation at different operating conditions. *Advances in Mechanical Engineering* 2019; 11: 1–12. DOI:10.1177/1687814019884780.
- [4] Hassan, H, Harmand, S. Effect of using nanofluids on the performance of rotating heat pipe. *Applied Mathematical Modelling* 2015; 39: 4445–62. DOI:https://doi.org/10.1016/j.apm.2014.12.023.
- [5] Hassan, H, Harmand, S. 3D transient model of vapour chamber: Effect of nanofluids on its performance.

- Applied Thermal Engineering* 2013; 51: 1191–201. DOI: <https://doi.org/10.1016/j.applthermaleng.2012.10.047>
- [6] C Calise, F, Figaj, RD, Vanoli, L. A novel polygeneration system integrating photovoltaic/thermal collectors, solar assisted heat pump, adsorption chiller and electrical energy storage: *Dynamic and energy-economic analysis. Energy Conversion and Management* 2017; 149: 798–814. DOI:10.1016/j.enconman.2017.03.027.
- [7] Gibelhaus, A, Fidorra, N, Lanzerath, F, Bau, U, Köhler, J, Bardow, A. Hybrid refrigeration by CO<sub>2</sub> vapour compression cycle and water-based adsorption chiller: An efficient combination of natural working fluids. *International Journal of Refrigeration* 2019; 103: 204–14. DOI:10.1016/j.ijrefrig.2019.03.036.
- [8] Lychnos, G, Tamainot-Telto, Z. Performance of hybrid refrigeration system using ammonia. *Applied Thermal Engineering* 2014; 62: 560–565. DOI:10.1016/j.applthermaleng.2013.10.013.
- [9] Cyklis, P. Two stage ecological hybrid sorption-compression refrigeration cycle. *International Journal of Refrigeration* 2014; 48: 121–131. DOI:10.1016/j.ijrefrig.2014.08.017.
- [10] Palomba, V, Varvagiannis, E, Karellas, S, Frazzica, A. Hybrid Adsorption-Compression Systems for Air Conditioning in Efficient Buildings: Design through Validated Dynamic Models. *Energies* 2019; 12(6). DOI:10.3390/en12061161.
- [11] Palomba, V, Lombardo, W, Große, A, Herrmann, R, Nitsch, B, Strehlow, A, Bastian, R, Sapienza, A, Frazzica, A. Evaluation of in-situ coated porous structures for hybrid heat pumps. *Energy* 2020; 209: 118313. DOI:10.1016/j.energy.2020.118313.
- [12] Vasta, S, Palomba, V, La, Rosa D, Mittelbach, W. Adsorption-compression cascade cycles: An experimental study. *Energy Conversion and Management* 2018; 156: 365–375. DOI:10.1016/j.enconman.2017.11.061.
- [13] Dino, GE, Palomba, V, Nowak, E, Frazzica, A. Experimental characterization of an innovative hybrid thermal-electric chiller for industrial cooling and refrigeration application. *Applied Energy* 2021; 281: 116098. DOI:10.1016/j.apenergy.2020.116098.
- [14] Kilic, M, Anjrini, M. Comparative performance analysis of a combined cooling system with mechanical and adsorption cycles. *Energy Conversion and Management* 2020; 221: 113208. DOI:10.1016/j.enconman.2020.113208.
- [15] Gado, MG, Megahed, TF, Ookawara, S, Nada, S, El-Sharkawy II. Performance and economic analysis of solar-powered adsorption-based hybrid cooling systems. *Energy Conversion and Management* 2021; 238: 114134. DOI:10.1016/j.enconman.2021.114134.
- [16] Koşan, M, Akkoç, AE, Dişli, E, Aktaş, M. Design of an innovative PV/T and heat pump system for greenhouse heating. *Journal of Energy Systems* 2020; 4: 58–70. DOI:10.30521/jes.740587.
- [17] Karaca, G, Dolgun, EC, Kosan, M, Aktas, M. Photovoltaic-Thermal solar energy system design for dairy industry. *Journal of Energy Systems* 2019; 3: 86–95. DOI:10.30521/jes.565174.
- [18] El-Sharkawy II, AbdelMeguid, H, Saha, BB. Potential application of solar powered adsorption cooling systems in the Middle East. *Applied Energy* 2014; 126: 235–45. DOI:10.1016/j.apenergy.2014.03.092.
- [19] Gado, MG, Megahed, TF, Ookawara, S, Nada, S, El-Sharkawy II. Energetic analysis of a PVT-based solar-driven hybrid adsorption-compression refrigeration system. In: ECRES 2021 9th Eur. Conf. Ren. Energy Sys.; 21-23 April 2021: dhepublisher, pp. 171–176.
- [20] Gado, MG, Nasser, M, Hassan, AA, Hassan, H. Adsorption-based atmospheric water harvesting powered by solar energy: Comprehensive review on desiccant materials and systems. *Process Safety and Environmental Protection* 2022; 160: 166–83. DOI:10.1016/J.PSEP.2022.01.061.
- [21] Gado, MG, Ookawara, S, Nada, S, Hassan, H. Renewable energy-based cascade adsorption-compression refrigeration system: Energy, exergy, exergoeconomic and enviroeconomic perspectives. *Energy* 2022:124127. DOI:<https://doi.org/10.1016/j.energy.2022.124127>.
- [22] Gado, MG, Megahed, TF, Ookawara, S, Nada, S, El-Sharkawy II. Parametric study of a hybrid adsorption-vapor compression cooling system. In: 3rd International conference of Chemical, Energy and Environmental Engineering, 27-28 July 2021: Alexandria, Egypt, pp. 1–6.
- [23] Saha, BB, Boelman, EC, Kashiwagi, T. Computer simulation of a silica gel-water adsorption refrigeration cycle - the influence of operating conditions on cooling output and COP. *ASHRAE Transactions* 1995; 101: 348–57.
- [24] Gado, MG, Elgendy, E, Elsayed, K, Fatouh, M. Parametric Study of an Adsorption Refrigeration System Using Different Working Pairs. *International Conference on Aerospace Sciences and Aviation Technology* 2017; 17: 1–15. DOI:10.21608/asat.2017.22455.
- [25] Gado, MG, Nada, S, Ookawara, S, Hassan, H. Energy management of standalone cascaded adsorption-compression refrigeration system using hybrid biomass-solar-wind energies. *Energy Conversion and Management* 2022; 258:115387. DOI:<https://doi.org/10.1016/j.enconman.2022.115387>.